NSD3-Induced Methylation of H3K36 Activates NOTCH Signaling to Drive Breast Tumor Initiation and Metastatic Progression

Ga-Young Jeong[1], Mi Kyung Park[2], Hee-Joo Choi[1,3], Hee Woon An[1], Young-Un Park[1], Hyung-Jun Choi[1], Jin Park[1], Hyung-Yong Kim[1], Taekwon Son[4], Ho Lee[2], Kyueng-Whan Min[1], Young-Ha Oh[1], Jeong-Yeon Lee[1,5], and Gu Kong[1,5]

ABSTRACT

Histone methyltransferase NSD3 is frequently dysregulated in human cancers, yet the epigenetic role of NSD3 during cancer development remains elusive. Here we report that NSD3-induced methylation of H3K36 is crucial for breast tumor initiation and metastasis. In patients with breast cancer, elevated expression of NSD3 was associated with recurrence, distant metastasis, and poor survival. *In vivo*, NSD3 promoted malignant transformation of mammary epithelial cells, a function comparable to that of HRAS. Furthermore, NSD3 expanded breast cancer-initiating cells and promoted epithelial–mesenchymal transition to trigger tumor invasion and metastasis. Mechanistically, the long isoform (full-length transcript) of NSD3, but not its shorter isoform lacking a catalytic domain, cooperated with EZH2 and RNA polymerase II to stimulate H3K36me2/3-dependent transactivation of genes associated with NOTCH receptor cleavage, leading to nuclear accumulation of NICD and NICD-mediated transcriptional repression of E-cadherin. Furthermore, mice harboring primary and metastatic breast tumors with overexpressed NSD3 showed sensitivity to NOTCH inhibition. Together, our findings uncover the critical epigenetic role of NSD3 in the modulation of NOTCH-dependent breast tumor progression, providing a rationale for targeting the NSD3–NOTCH signaling regulatory axis in aggressive breast cancer.

Significance: This study demonstrates the functional significance of histone methyltransferase NSD3 in epigenetic regulation of breast cancer stemness, EMT, and metastasis, suggesting NSD3 as an actionable therapeutic target in metastatic breast cancer.

Introduction

Distant metastasis of breast cancer, which is a major cause of cancer-related death, is still regarded as incurable with currently available therapies (1). Cancer stem cells (CSC), a small subset of cancer cells capable of initiating tumors with stem cell-like characteristics, are known as a major contributor to tumor relapse and metastasis (2). Accumulating evidence also indicates that epithelial–mesenchymal transition (EMT), a process of initial step for tumor metastasis whereby epithelial cells undergo a mesenchymal phenotypic change to adopt migratory and invasive abilities (3), is crucial for the generation of breast CSC-like cells (4–7), prompting the need for CSC/EMT-directed therapy for metastatic breast cancer. Notably, reversible epigenetic changes have been implicated in the phenotypic plasticity of CSCs and EMT (8, 9). An increasing number of studies by our and other research groups has shown that several histone methyltransferases/demethylases (HMT/HDM) targeting H3K4, H3K9, H3K27, and H3K79, play a critical role in the acquisition and maintenance of CSCs and/or EMT (8–13). Furthermore, recent genome-wide analyses have found frequent genetic aberrations of multiple HMTs in human cancers (14, 15), implying that the altered enzymatic activities of these HMTs may be involved in the tumor initiation and metastasis as potential regulators of CSCs and EMT.

Nuclear receptor binding SET domain protein 3 (NSD3/WHSC1L1) belongs to the NSD family of lysine methyltransferases that mainly catalyze histone H3 lysine 36 di- and trimethylation (H3K36me2/3; ref. 16). It was originally identified as a frequently amplified gene mapped to chromosome 8p12 in breast cancer (17), and has been reported to be overexpressed in various human cancers, including lung and pancreatic cancers (14, 18–20). There are two representative isoforms of NSD3, the full-length transcript and shorter isoform lacking a catalytic SET domain, designated as NSD3-long and NSD3-short, respectively, found in mammalian cells (17, 21). Although the HMT activity-independent molecular function of NSD3-short has been reported in human leukemia and breast cancer cells (22, 23), little is known about the role of NSD3-long in human cancers; thus, it remains unclear whether NSD3-induced histone methylation is functionally important in cancer initiation and progression.

In this study, we comprehensively explored the role of NSD3 in breast cancer, a type of cancer with high frequency of *NSD3* gene amplification and uncovered that NSD3 has potential to promote malignant transformation of breast epithelial cells, and tumor-initiating and metastatic capacities of cancer cells. The NSD3 catalytic activity toward H3K36 was linked to the activation of NOTCH signaling and a subsequent induction of EMT and CSCs. Taken

[1]Department of Pathology, College of Medicine, Hanyang University, Seoul, Republic of Korea. [2]Department of Cancer Biomedical Science, Graduate School of Cancer Science and Policy, National Cancer Center, Goyang, Gyeonggi, Republic of Korea. [3]Institute for Bioengineering and Biopharmaceutical Research (IBBR), Hanyang University, Seoul, Republic of Korea. [4]College of Pharmacy, Seoul National University, Seoul, Republic of Korea. [5]Department of HY-KIST Bio-convergence, Hanyang University, Seoul, Republic of Korea.

Note: Supplementary data for this article are available at Cancer Research Online (http://cancerres.aacrjournals.org/).

G.-Y. Jeong, M.K. Park, and H.-J. Choi contributed equally to this article.

Corresponding Authors: Gu Kong, Hanyang University, 17 Haengdang-dong, Seongdong-gu, Seoul 133-791, Republic of Korea. Phone: 82-2-2290-8251; Fax: 82-2-2295-1091; E-mail: gkong@hanyang.ac.kr; and Jeong-Yeon Lee, E-mail: jy2jy2@hanyang.ac.kr

Cancer Res 2021;81:77–90

doi: 10.1158/0008-5472.CAN-20-0360

together, these findings propose a crucial role of NSD3-induced H3K36 methylation in breast tumor initiation and metastasis, suggesting NSD3 as a potential therapeutic target for aggressive breast cancer.

Materials and Methods

Patients, surgical specimens, and IHC

For IHC analysis of NSD3 expression in human breast cancers, primary tumor tissues obtained from 230 patients with breast cancer diagnosed with invasive ductal carcinoma at Hanyang University Hospital between 2000 and 2009 were used under the approval of Institutional Review Boards of Hanyang University (Seoul, Republic of Korea). Paraffin-embedded and formalin-fixed tumor tissue microarrays (TMA) specimens were immunostained with a primary antibody against NSD3 (1:100, 11345–1-AP; Proteintech) using the Dako Autostainer Universal Staining System (Dako) and the ChemMate DAKO EnVision Detection Kit (Dako). Of the 230 cases, 29 cases were excluded due to the unavailability of paraffin blocks or inadequate clinical history. The intensity of immunostaining was recorded as follows: 0 (no staining), 1 (weak), 2 (moderate), and 3 (strong). The proportion of staining was graded as follows: 0 (0–5%), 1 (6–25%), 2 (26–50%), 3 (51–75%), and 4 (>75%). Immunoreactive score (IRS) was calculated (intensity × proportion), and IRS > 3 was considered as a positive case for NSD3 expression.

Cell culture and reagents

HuMEC, MCF10A, MCF7, T47D, MDA-MB-231, and JIMT1 cells were obtained from the ATCC. ZR-75–1 and HCC-1599 cells were purchased from Korean Cell Line Bank. MCF7, T47D, MDA-MB-231, and 293T cells were cultured in DMEM (Welgene) supplemented with 10% FBS, and HCC-1599 and JIMT1 cells were cultured in RPMI (Welgene) supplemented with 10% FBS at 37°C in a 5% CO_2 atmosphere. MCF10A human breast epithelial cells and MCF10AT cell line, generated by lentiviral transduction of HRAS into wild-type MCF10A cells, were maintained in DMEM/F12 medium (Welgene) supplemented with 5% horse serum, 20 ng/mL EGF, 10 μg/mL insulin, and 0.5 μg/mL hydrocortisone. Cell lines were tested for mycoplasma contamination by Mycoplasma PCR Detection Kit (iNtRON bio). Cell lines were used for less than 50 passages, but were not independently authenticated. For pharmacologic inhibition of NOTCH signaling, a γ-secretase inhibitor (GSI), RO4929097, was purchased from MedChem Express.

Mammosphere and tumorsphere formation assay

MCF10A (1.5×10^4 cells/well) cells were cultured in DMEM-GlutaMAX medium (Invitrogen) supplemented with 2% B27 (Invitrogen), 20 ng/mL basic FGF (bFGF; Peprotech), 20 ng/mL EGF, 5 μg/mL insulin (Sigma-Aldrich), and 4 μg/mL heparin (Sigma-Aldrich) in a six-well ultra-low attachment surface plate (Corning). MCF7 (1×10^4 cells/well), T47D (5×10^3 cells/well), ZR-75–1 (1×10^4 cells/well), and MDA-MB-231 (5×10^3 cells/well) cells were cultured in the same medium as above without insulin, and JIMT1 (1×10^4 cells/well) cells were cultured in DMEM-GlutaMAX medium supplemented with 2% B27, 20 ng/mL bFGF, 20 ng/mL EGF, 5 μg/mL insulin, 4 μg/mL heparin, and 0.5 μg/mL hydrocortisone (Sigma-Aldrich), in a six-well ultra-low attachment surface plate. The formation of primary and secondary spheres at the indicated days was measured and quantified as described previously (24).

Soft-agar colony formation assay

For anchorage-independent colony formation, 0.8% agar (Difco) in a growth medium was precoated on six-well plates, and MCF7 and MDA-MB-231 cells (1×10^4 and 2.5×10^3 cells per well, respectively) mixed with a medium containing 0.7% agar were then spread on top of the base agar layer. The cells were treated with either a vehicle (DMSO) or RO4929097 twice per week. After 21 days of incubation, colonies were stained with 0.5% crystal violet (Sigma-Aldrich) and washed with PBS. The stained colonies were then counted and photographed using the inverted phase microscope (Carl Zeiss).

Orthotopic tumor xenografts

All mouse experiments were approved and performed in accordance with the Institutional Animal Care and Use Committee of the Hanyang University (Seoul, Republic of Korea) and National Cancer Center (Goyang, Gyeonggi, Republic of Korea). Five-week-old female NOD/SCID mice were purchased from KOATECH, Korea Research Institute of Bioscience and Biotechnology (KRIBB), or Charles River Laboratories Japan, Inc., for use in the following experiments. For all the experiments, tumor size was measured twice per week by using a caliper. The tumor volume was calculated as follows: Volume (mm^3) = $(a \times b^2)/2$, where "a" and "b" indicate the largest and perpendicular diameters, respectively.

Malignant transformation and tumor initiation

To investigate the malignant transformation of mammary epithelial cells in response to HRAS and NSD3 isoforms, 1×10^6 MCF10A or MCF10AT cells (HRAS-transduced MCF10A cells) stably expressing either NSD3-short or NSD3-long were injected into the mammary fat pads of NOD/SCID mice. Tumor formation and growth in each mouse were monitored for 84 days. For measurement of *in vivo* tumor-initiating ability, serially diluted NSD3-overexpressing MCF7 cells or NSD3-knockdown MDA-MB-231-luc-D3H2LN cells, resuspended in Matrigel (BD Biosciences), were orthotopically injected into mice. The E2 pellets (0.72 mg/pellet; 60-day release; Innovative Research of America) were implanted 1 week before MCF7 cell injection. The frequency of tumor formation was analyzed using the L-Calc software (Stemcell Technologies).

Tumor growth and metastasis

To determine the effect of NSD3 on breast cancer progression and metastasis in an orthotopic xenograft model, 2×10^6 MDA-MB-231-luc-D3H2LN cells stably expressing either control- or NSD3 shRNA were resuspended in Matrigel, and injected into mammary fat pads of mice. The mice were injected intraperitoneally with D-luciferin (Xenogen) once every week to measure luciferase activity using the IVIS 200 imaging system (Xenogen). Mice were sacrificed 12 weeks after the cell injection, and primary tumors and lungs from each mouse were fixed in formalin, and paraffin-embedded for histologic analyses. The tumor area of lung tissues was measured with the software AxioVision.

Anticancer effect of γ-secretase inhibitor treatment *in vivo*

To examine the inhibitory effect of RO4929097, a GSI, on NSD3-induced breast tumor growth in an orthotopic xenograft model, 1×10^6 MDA-MB-231 cells stably overexpressing NSD3 or 2×10^6 MDA-MB-231 cells with stable NSD3-knockdown followed by the restored NSD3-long and NICD1 expression were injected orthotopically into mammary fat pads of mice. When the tumor volume reached approximately 100 mm^3 in size, RO4929097 (10 and 30 mg/kg) was administrated orally for 2 to 3 weeks (5 days on/2 days off) to the mice.

To investigate the effect of pharmacologic inhibition of NOTCH signaling on NSD3-induced tumor metastasis, 1×10^6 NSD3-overexpressing MDA-MB-231 cells or 2×10^6 NSD3-knockdown

MDA-MB-231 cells with the restoration of NSD3-long or NICD1 were injected into the tail vein of NOD/SCID mice. The mice were treated with 10 or 30 mg/kg RO4929097 by oral gavage as described above and sacrificed at 3 weeks postinjection to quantify lung metastatic colonization by histologic analysis. The tumor area of lung tissues was measured using the AxioVision software.

Data availability

The RNA-sequencing (RNA-seq) data have been deposited to the Gene Expression Omnibus (GEO) database under the accession number GSE152546.

Results

NSD3 is a cancer driver associated with poor clinical outcome in breast cancer

To demonstrate the clinical implication of NSD3 in breast cancer, we first investigated the genetic alterations of NSD family in patients with cancer. In the METABRIC and TCGA breast cancer datasets, aberrant copy numbers and expression of *NSD3* were found in approximately 15% to 20% of breast cancers, whereas other NSD family members, *NSD1* and *NSD2*, had very low frequency of genetic alterations (≤5%; **Fig. 1A**). Among the *NSD3* genetic aberrations, the prevalence of *NSD3* amplification was relatively higher in breast cancer, as well as in lung squamous cell carcinomas, and bladder cancer, than in other types of cancers (Supplementary Fig. S1A). *NSD3* amplification, accounting for around 13% of breast cancers, was associated with worse overall survival (OS; TCGA, $P = 0.031$; METABRIC, $P = 0.005$) and disease-free survival (DFS; METABRIC, $P = 0.005$; **Fig. 1B**; Supplementary Fig. S1B). The copy numbers of *NSD3* strongly correlated with its gene expression (Supplementary Fig. S1C; TCGA, Pearson's $r = 0.85$; METABRIC, Pearson's $r = 0.83$), and the elevated *NSD3* mRNA and protein levels were associated with poorer survival outcomes in patients with breast cancer from the METABRIC (OS, $P = 0.009$; DFS, $P = 0.020$) and our cohorts (OS, $P = 0.009$; DFS, $P = 0.011$), respectively (**Fig. 1C** and **D**; Supplementary Fig. S1D). When comparing the clinical impact of two NSD3 isoforms using TCGA dataset, high expression levels of either NSD3-long or NSD3-short exhibited a tendency toward shorter OS and DFS, but only the prognostic value of NSD3-long was statistically significant (OS, $P = 0.045$; DFS, $P = 0.043$; **Fig. 1E**). These isoforms had similar expression patterns across breast cancer subtypes in the patients (Supplementary Fig. S1E). Together, these findings suggest that high *NSD3* amplification/expression is a prognostic marker for poor outcome in breast cancer.

On the basis of the information on the CCLE dataset indicating the genetic alterations and expression levels of *NSD3* in different subtypes of human breast cancer cells (**Fig. 1F**), we next examined the expression pattern of each isoform of NSD3 in several breast cancer cell lines with or without *NSD3* gene amplification. NSD3-long and NSD3-short were concurrently expressed in these cell lines, with the elevated levels compared with human mammary epithelial cells (HuMEC) and immortalized MCF10A cells (**Fig. 1G**). Consistently, *NSD3* was highly expressed in breast cancer tissues compared with adjacent normal tissues in the patients (TCGA, $P < 0.001$; METABRIC, $P < 0.001$; Supplementary Fig. S1F), implying that NSD3 may contribute to breast tumorigenicity. NSD3-short isoform was previously reported to transform MCF10A immortalized mammary epithelial cells in 2D and 3D cultures (23), but no direct evidence *in vivo* is yet known. To verify the malignant potential of each NSD3 isoform *in vivo*, the tumor-forming abilities of MCF10A and MCF10AT (HRAS-transfected MCF10A) cells stably expressing either the NSD3-long- or NSD3-short isoform were evaluated in orthotopic xenograft mice. Although there was no apparent tumor generated in the control mice, both NSD3-long- and NSD3-short-expressing mice developed tumors, and the malignant capacity of NSD3-long was greater than that of NSD3-short, and comparable to the ability of HRAS (**Fig. 1H–J**). The coexpression of NSD3-long and HRAS additively promoted the tumor-forming ability. These results indicated that both NSD3 isoforms enable to potentiate the malignant transformation of breast epithelial cells, and the higher transforming ability of NSD3-long than that of NSD3-short may reflect the functional importance of NSD3 enzymatic activity in breast tumorigenesis.

NSD3 induces CSC-like properties for breast tumor initiation

To elucidate the functional relevance of NSD3 in breast cancer, lentiviral overexpression of NSD3 full-length transcript and RNAi-mediated knockdown of NSD3 were established in several breast cancer cells displaying low and moderate/high endogenous expression levels of NSD3 isoforms, respectively (**Fig. 1G**; Supplementary Figs. S2A and S2B). In the gene set enrichment analysis (GSEA) of the RNA-seq results from MDA-MB-231 cells with shRNA-mediated NSD3 knockdown, the altered genes by NSD3 depletion were associated with gene sets linked to stem/progenitor cells, proliferation, tumor invasion, metastasis, and high-grade tumors (**Fig. 2A** and **B**). In accordance with these observations, NSD3 was involved in the acceleration of tumor growth both *in vitro* and *in vivo* (Supplementary Figs. S2C and S2D). Furthermore, the overexpression of NSD3 increased the $CD44^+/CD24^-/ESA^+$ cells, a population of breast CSCs (25), and the ability to form tumorspheres in serial passages in MCF10A and MCF7 cells (**Fig. 2C** and **D**; Supplementary Figs. S3A and S3B), whereas NSD3 knockdown suppressed these CSC-like properties in T47D and MDA-MB-231 cells harboring high and moderate NSD3 expression levels, respectively, without *NSD3* gene amplification (**Figs. 1G**, **2C** and **D**; Supplementary Figs. S2A and S2B). Similarly, in *NSD3*-amplified JIMT1 and ZR-75-1 cells, NSD3 depletion exhibited impaired CSC-like phenotype (**Fig. 2C** and **D**; Supplementary Figs. S3C–S3E). In ZR-75-1 cells, no detectable $CD44^+/CD24^-/ESA^+$ cell population was observed, but the tumorsphere-forming ability was inhibited by NSD3 knockdown (Supplementary Figs. S3D and S3E). Consistently, *in vivo* limiting dilution assay showed that NSD3 overexpression increased the tumor-initiating frequency in mice orthotopically injected with MCF7 tumors (**Table 1**; Supplementary Fig. S3F; top). Likewise, mice harboring NSD3-knockdown MDA-MB-231 tumors exhibited decreased tumor-initiating ability, compared with the control mice (**Table 1**; Supplementary Fig. S3F; bottom). These data demonstrated that NSD3 maintains CSC-like properties for breast tumor initiation and progression.

We further compared the effect of NSD3-long and NSD3-short isoforms on the self-renewal of CSC-like cells in various stable cell lines manipulating the expression levels of these isoforms. In MCF7 cells with low endogenous levels of NSD3 isoforms, overexpression of either NSD3-long or NSD3-short enhanced CSC-like cell population and sphere-forming ability, and coexpression of both NSD3 isoforms addictively increased these effects (Supplementary Figs. S4A–S4C). In MDA-MB-231, JIMT1, and ZR-75-1 cells expressing both NSD3 isoforms, NSD3-long-specific knockdown was able to inhibit the CSC-like phenotype at a level similar to or lower than the dual knockdown effect of NSD3-long and -short (Supplementary Figs. S4A–S4C). Furthermore, the restoration of NSD3-long and NSD3-short in NSD3 shRNA-transduced MDA-MB-231 cells recovered tumorsphere-forming ability impaired by the NSD3 knockdown (Supplementary

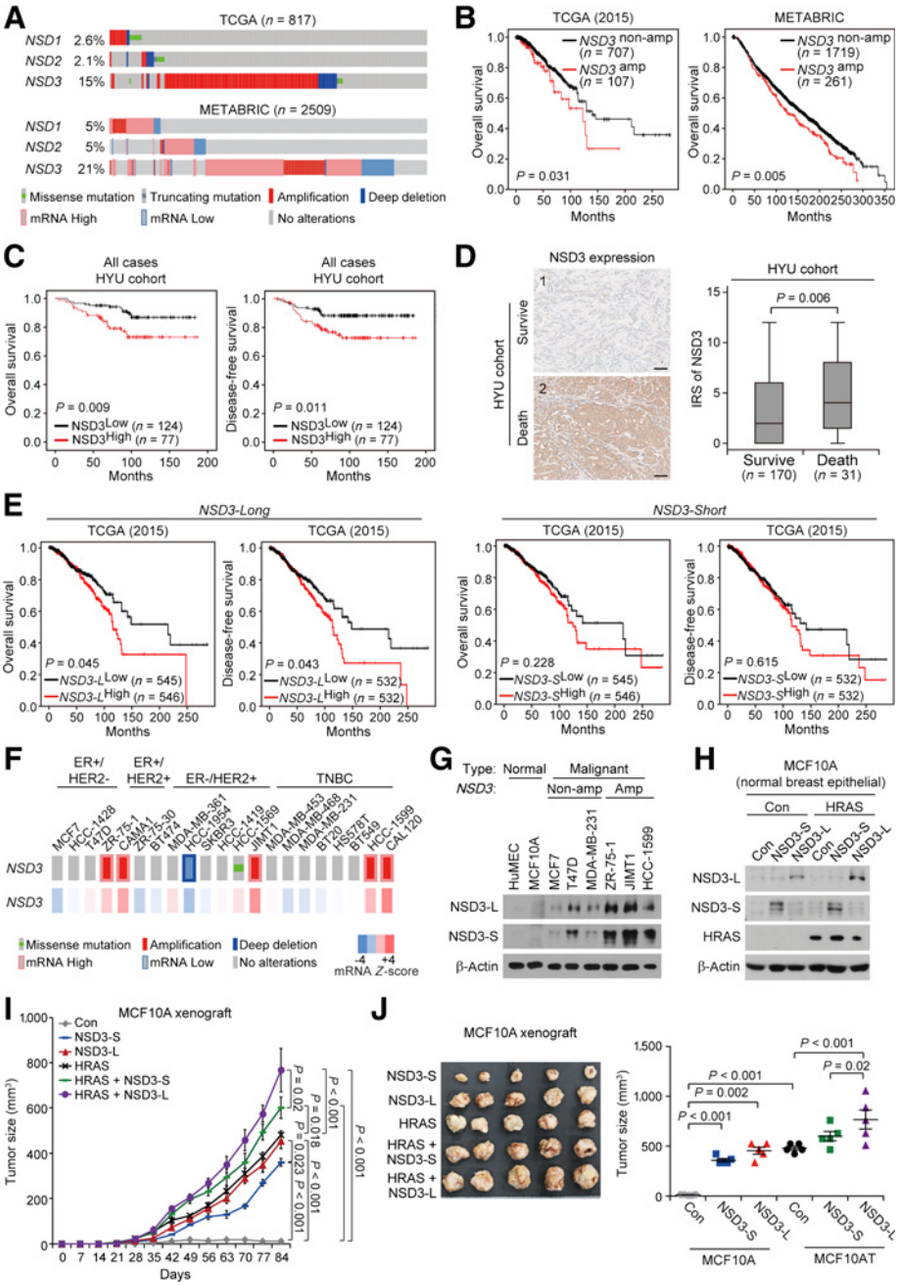

Figure 1.

Clinical implication and cancer-driving role of NSD3 in breast cancer. **A,** Oncoprints representing the genetic alterations of NSD family members in the indicated breast cancer datasets. **B,** OS analysis of patients with breast cancer according to the *NSD3* amplification status in the indicated datasets. *P* values were calculated using the Kaplan–Meier method with the log-rank test. amp, amplification, non-amp, nonamplification. **C,** Analysis of OS and DFS of patients with breast cancer according to NSD3 expression in our cohort (HYU, Hanyang University). Groups were stratified by IHC-based NSD3 protein expression. *P* values were calculated using the Kaplan–Meier method with the log-rank test. **D,** IHC analysis of NSD3 expression levels in the indicated groups from our breast cancer cohort. Scale bar, 100 μm. *P* value was calculated using two-sided Student *t* test. **E,** OS and DFS analysis of patients with breast cancer according to NSD3-long (NSD3-L) and NSD3-short (NSD3-S) expression in the TCGA. *P* values were calculated using the Kaplan–Meier method with the log-rank test. **F,** Oncoprints representing the genetic alterations and relative expression levels of *NSD3* in the indicated subtypes of breast cancer cell lines from CCLE dataset. **G,** Immunoblot analysis showing the NSD3 expression levels in the indicated breast cancer cell lines with or without *NSD3* gene amplification. Amp, *NSD3* amplification; Non-amp, nonamplification of *NSD3*. **H,** Generation of MCF10A and MCF10AT (HRAS-overexpressing MCF10A) cell lines stably expressing either NSD3-L or NSD3-S as confirmed by immunoblotting. **I** and **J,** The effect of NSD3 isoforms on the malignant transformation of MCF10A cells *in vivo*. **I,** The growth curve of tumors generated from mice orthotopically xenografted with indicated stable cell lines. Mean ± SEM ($n = 5$ mice per group). *P* values were calculated using RM ANOVA with a *post hoc* LSD test. **J,** Left, images of tumors from mice sacrificed on the final day. Right, graphs showing the tumor volumes of each group at last time point. Mean ± SEM ($n = 5$). *P* value was determined by one-way ANOVA with Dunnett's T3 test.

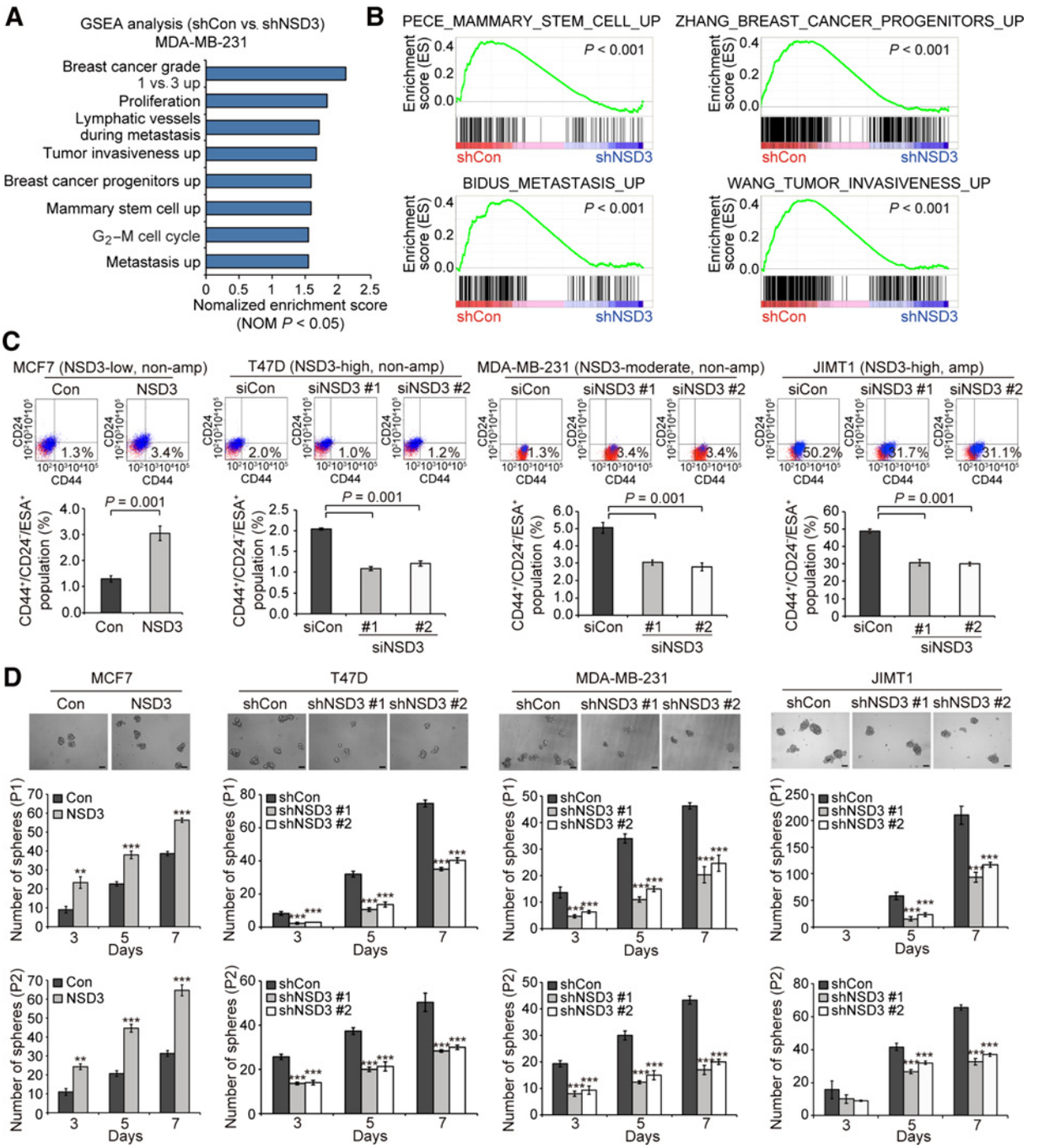

Figure 2.

NSD3 effect on breast CSC-like properties. **A** and **B,** GSEA showing the enrichment of indicated gene signatures in control MDA-MB-231 cells (shCon) compared with NSD3-knockdown (shNSD3) cells from RNA-seq analysis. **C,** FACS analysis of $CD44^+/CD24^-/ESA^+$ cells in breast cancer cell lines stably overexpressing NSD3 or transiently knocked down NSD3. Representative dot plots of CD44-APC versus CD24-PE expression for variable cells (P1 gate, red) and for ESA^+ cells (P2 gate, blue) from P1 gate. Bar graphs indicate the percentage of $CD44^+/CD24^-/ESA^+$ cell population in the indicated groups. Mean ± SD ($n = 3$). *P* values by two-sided Student *t* test (MCF7) or one-way ANOVA with a *post hoc* LSD test (T47D, MDA-MB-231, and JIMT1). Con, control; NSD3, NSD3 overexpression; siCon, negative control (nontargeting scrambled siRNA); siNSD3, NSD3 siRNA. **D,** Tumorsphere formation analysis in the indicated group of cell lines. Representative images of primary tumorspheres are displayed (top). Scale bar, 100 μm. The primary (P1) and secondary (P2) tumorspheres formed at 3, 5, 7 days were counted and are represented as bar graphs. Mean ± SD ($n = 3$). *P* values by two-sided Student *t* test (MCF7) or one-way ANOVA with a *post hoc* LSD test (T47D, MDA-MB-231, and JIMT1). **, $P < 0.01$; ***, $P < 0.001$ versus controls (Con or shCon).

Table 1. NSD3 enhances *in vivo* tumor-initiating ability.

Cell type	Cell number for injection	Days				
		21 days	25 days	28 days	32 days	35 days
MCF7	500	0/7	0/7	0/7	0/7	0/7
Con	1,000	0/7	0/7	0/7	0/7	1/7
	5,000	0/7	1/7	1/7	3/7	5/7
	10,000	0/7	1/7	4/7	7/7	7/7
TIC frequency			1/53,903 (1/13,457–1/215,922)	1/18,213 (1/7,658–1/43,316)	1/6,315 (1/3,368–1/11,839)	1/3,967 (1/2,177–1/7,229)
MCF7	500	0/7	0/7	0/7	0/7	2/7
NSD3	1,000	0/7	1/7	1/7	3/7	4/7
	5,000	2/7	4/7	7/7	7/7	7/7
	10,000	3/7	6/7	7/7	7/7	7/7
TIC frequency		1/18,791 (1/7,817–1/45,171)	1/5,962 (1/3,200–1/11,111)	1/2,582 (1/1,394–1/4,784)	1/1,911 (1/1,001–1/3,648)	1/1,190 (1/598–1/2,369)
P value			0.005	<0.001	0.009	0.010

Cell type	Cell number for injection	Days				
		14 days	17 days	21 days	24 days	28 days
MDA-MB-231	500	0/6	0/6	1/6	2/6	4/6
shCon	1,000	0/6	0/6	4/6	4/6	5/6
	5,000	0/6	4/6	6/6	6/6	6/6
	10,000	4/6	5/6	6/6	6/6	6/6
TIC frequency		1/19,321 (1/7,414–1/50,350)	1/6,254 (1/3,176–1/12,317)	1/1,196 (1/569–1/2,514)	1/989 (1/467–1/2,091)	1/507 (1/245–1/1,049)
MDA-MB-231	500	0/6	0/6	0/6	0/6	0/6
shNSD3	1,000	0/6	0/6	0/6	1/6	3/6
	5,000	0/6	0/6	3/6	5/6	6/6
	10,000	0/6	2/6	5/6	6/6	6/6
TIC frequency			1/44,312 (1/11,264–1/174,328)	1/7,538 (1/3,728–1/15,243)	1/3,311 (1/1,728–1/6,345)	1/1,762 (1/868–1/3,575)
P value			0.012	0.001	0.017	0.016

Note: For *in vivo* limiting dilution assays, serially diluted MCF7 cells stably overexpressing NSD3 or control (Con) and MDA-MB-231 cells expressing either control shRNA (shCon) or NSD3 shRNA (shNSD3) were injected into the mammary fat pads of NOD/SCID mice. The tumor-initiating cell (TIC) frequency was calculated using L-Calc software (Stemcell Tech, http://www.stemcell.com).

Fig. S4D). These data indicated that both NSD3-short and NSD3-long are crucial for the maintenance of breast CSCs.

NSD3 promotes EMT and tumor metastasis in breast cancer

As EMT can induce CSC-like properties and tumor metastasis (4–7, 26, 27), we next examined the effect of NSD3 on EMT phenotype. In MCF10A and MCF7 epithelial cells, NSD3 overexpression induced EMT morphologic changes, accompanied by loss of epithelial marker E-cadherin and gain of mesenchymal markers, Vimentin and N-cadherin (**Fig. 3A–C**). Moreover, the expression of basal marker keratin 14 was upregulated, whereas the expression of luminal marker keratin 19 slightly decreased in NSD3-overexpressing MCF7 cells (Supplementary Figs. S5A and S5B), indicating the luminal-to-basal switch in response to NSD3. In MCF10A and MDA-MB-231 cells showing high levels of keratin 14 and 19, respectively, NSD3 overexpression and knockdown did not affect the expression levels of these keratins. Subsequently, NSD3 overexpression triggered migration and invasion of these cells (**Fig. 3D** and **E**; Supplementary Fig. S6A, left). Likewise, NSD3 knockdown in MDA-MB-231 mesenchymal-like breast cancer cells led to the reversal of EMT (**Fig. 3A–C**), and impaired migration and invasion abilities (**Fig. 3D** and **E**). In *NSD3*-amplified JIMT1 cells, NSD3 knockdown also suppressed migration and invasion abilities (Supplementary Fig. S6A, right). In addition, NSD3 inhibited *CDH1* (encoding E-cadherin) transcription, whereas it positively modulated the expression of Snail and Slug, key transcriptional repressors of *CDH1* (4) in various NSD3 stable cell lines (Supplementary Figs. S6B–S6E). When comparing the effect of NSD3-long and -short isoforms on EMT-like phenotype, both NSD3 isoforms were involved in the regulation of invasion/migration capacities and EMT marker expression, and the ability of NSD3-long was greater than that of NSD3-short (Supplementary Figs. S6F and S6G). Furthermore, mice harboring MDA-MB-231 breast tumor with stable knockdown of NSD3 isoforms exhibited suppression of tumor progression and metastasis to the lungs (**Fig. 3F** and **G**), which was consistent with the clinical evidence for the association between NSD3 expression and tumor recurrence caused by distant metastasis in the survival analysis (**Fig. 3H**). Thus, these results suggested that NSD3 promotes metastatic progression of breast tumor as a regulator of CSCs and EMT.

NSD3 triggers ADAM12-mediated NOTCH receptor cleavage and activates NOTCH signaling to modulate EMT regulators

To identify the molecular mechanism underlying the regulation of breast CSCs/EMT by NSD3, we next explored signaling pathways where NSD3-target genes are mainly involved. The GSEA of RNA-seq results indicated that NSD3-target genes were enriched for WNT, AKT/PKB, HRAS, EZH2, and NOTCH signaling, which are major pathways of CSCs, EMT, and metastasis (4) (**Fig. 4A**). Particularly,

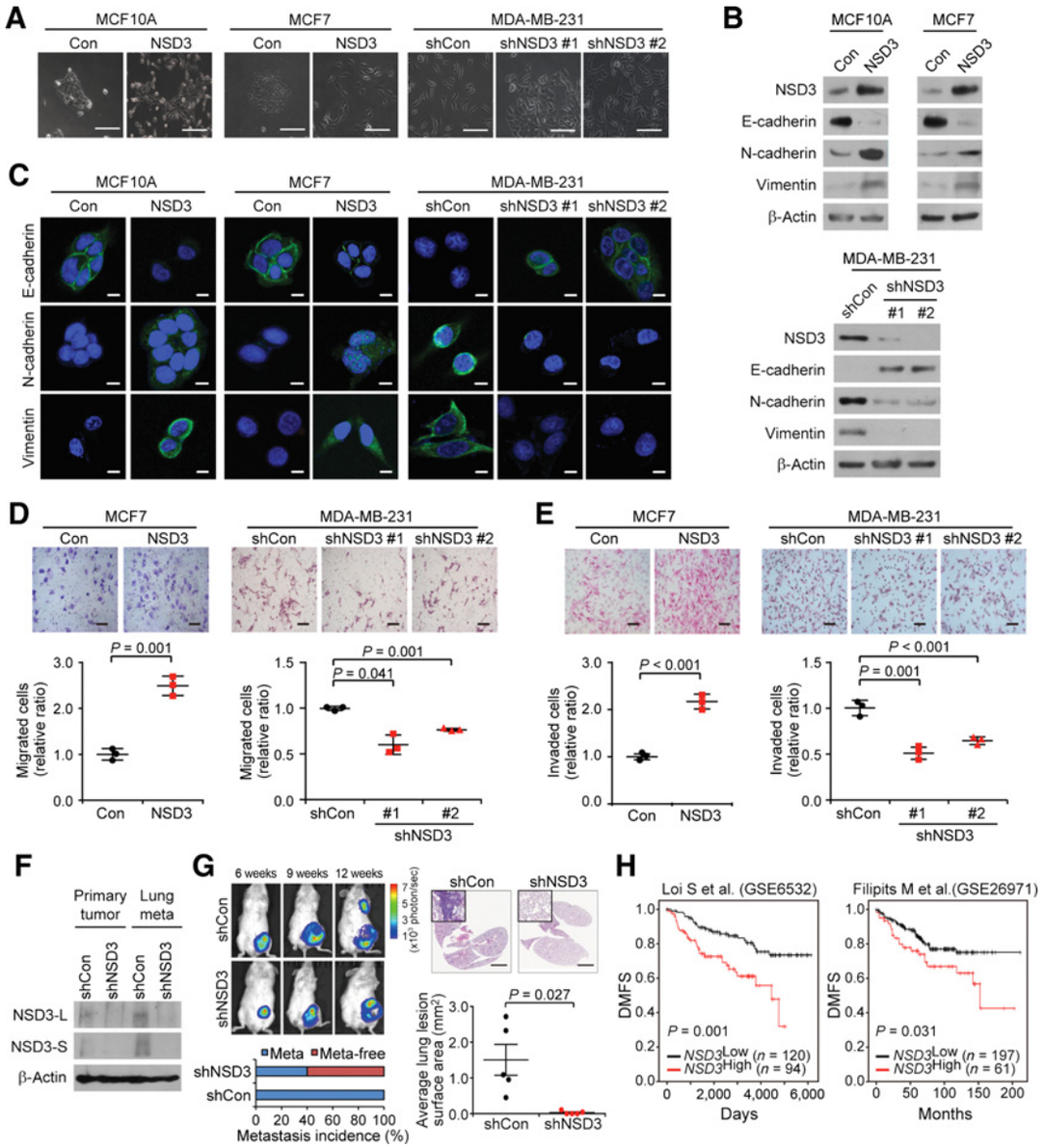

Figure 3.

NSD3 effect on EMT and tumor metastasis in breast cancer. **A,** Morphologic changes in the indicated cells in response to NSD3 expression evaluated by microscopy. Scale bars, 100 μm. **B,** Immunoblot analysis showing changes in the expression levels of epithelial and mesenchymal markers by NSD3 overexpression (top) or NSD3 knockdown (bottom). **C,** Immunofluorescence images for the expression of epithelial and mesenchymal markers (green) in the indicated stable cell lines. DAPI (blue) was used for the visualization of nucleus. Scale bars, 10 μm. **D** and **E,** Analysis of migration (**D**) and invasion (**E**) ability of breast cancer cell lines in response to NSD3 overexpression (left) or knockdown (right). Mean ± SD ($n = 3$). *P* values are based on two-sided Student *t* test (MCF7) and one-way ANOVA with a *post-hoc* LSD (invasion, MDA-MB-231) or Dunnett's T3 test (migration, MDA-MB-231). Scale bars, 100 μm. **F,** Immunoblot analysis indicating the expression levels of NSD3 isoforms in tumor tissues from primary and lung metastatic sites of mice injected with MDA-MB-231-luc-D3H2LN cells stably expressing either control shRNA (shCon) or NSD3 shRNA (shNSD3). Lung meta, lung metastasis. **G,** Effect of NSD3 on lung metastasis of breast cancer in xenografted mice. Top left, bioluminescence images at the indicated weeks after orthotopic injection of control (shCon) or NSD3-knockdown (shNSD3)-MDA-MB-231-luc-D3H2LN cells into mice. Top right, representative hematoxylin and eosin–stained lung sections from the indicated group of mice for analysis of metastatic colonization. The results were quantified by measuring the incidence of lung metastasis (bottom left) and tumor area of lung tissues from mice (bottom right). Mean ± SEM ($n = 5$). *P* value was calculated using two-sided Student *t* test (bottom right). Meta, metastasis; Meta-free, metastasis-free. **H,** Analysis of distant metastasis-free survival (DMFS) of patients with breast cancer from indicated datasets based on the *NSD3* mRNA levels. *P* values were determined by the Kaplan–Meier method with the log-rank test.

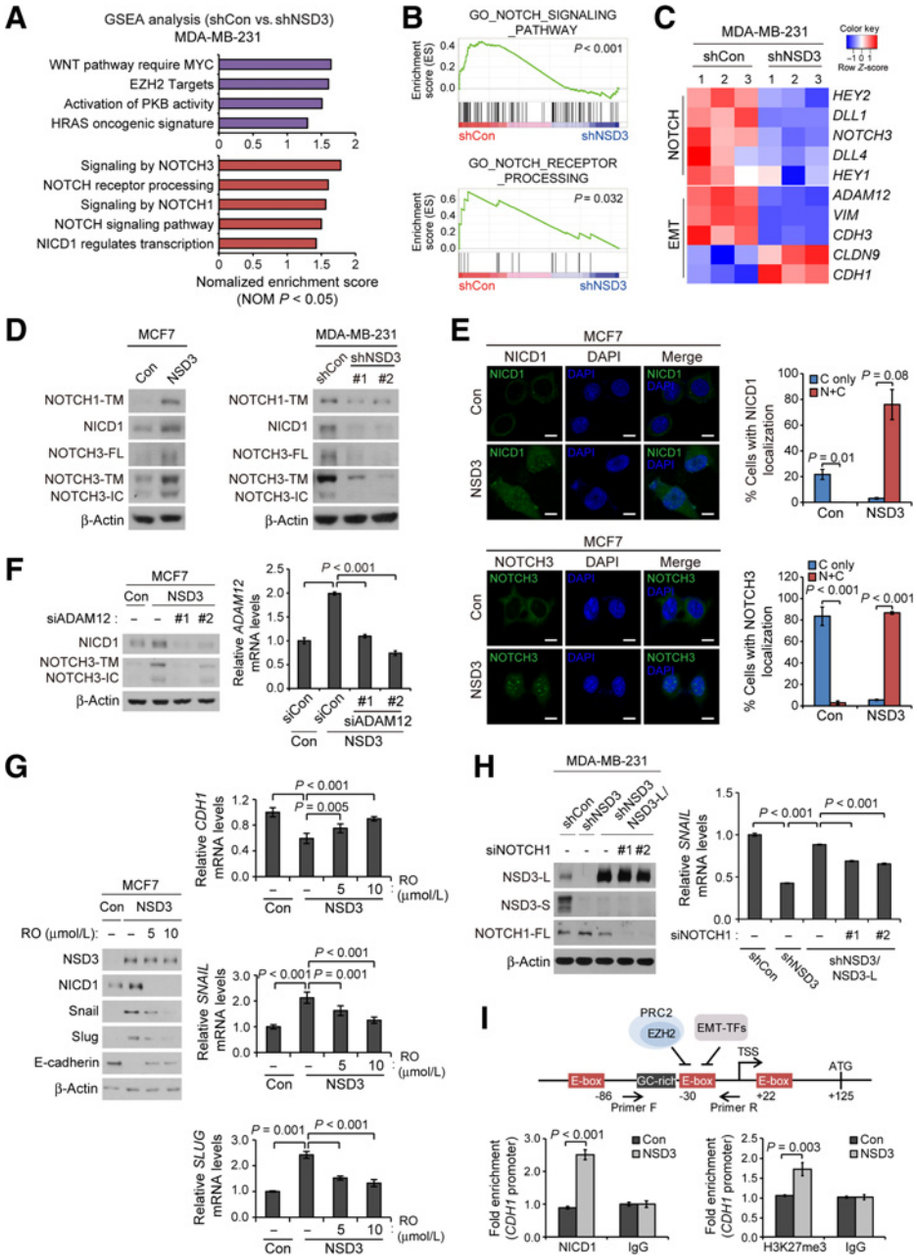

Figure 4.

Regulation of NOTCH receptor cleavage and signaling activation by NSD3. **A** and **B,** GSEA of RNA-seq data to analyze signaling pathways altered by NSD3 knockdown in MDA-MB-231 cells. **C,** Heatmap showing changes in the expression of indicated genes by the NSD3 knockdown. **D,** Immunoblot analysis of the expression levels of full length (FL)- and cleaved NOTCH receptors (TM, transmembrane; IC, intracellular) in the indicated stable cell lines. **E,** Immunofluorescence staining of NICD1 and NOTCH3 for measuring the subcellular localization of NOTCH receptors in response to NSD3 expression in MCF7 cells. Data were quantified by counting the cells harboring exclusively cytoplasmic NOTCH receptors (C only) or cells coexpressing both cytoplasmic and nuclear NOTCH receptors (C+N). Mean ± SD ($n = 3$). *P* values are based on two-sided Student *t* test. **F,** NSD3-overexpressing MCF7 cells were treated with ADAM12 siRNA for 48 hours and changes in the expression of *ADAM12* and cleaved NOTCH receptor were analyzed by immunoblotting (left) and qRT-PCR (right). Mean ± SD ($n = 3$). *P* values were calculated using one-way ANOVA with a *post hoc* LSD test. **G,** Effect of NOTCH signaling inhibition on EMT markers/regulators expression. NSD3-overexpressing MCF7 cells were treated with indicated doses of RO4929097 (RO), a GSI, for 24 hours, and subjected to immunoblotting (left) and qRT-PCR (right) for analysis of NOTCH signaling effect on NSD3-induced EMT. Mean ± SD ($n = 3$). *P* values are based on one-way ANOVA, followed by a *post hoc* LSD (*CDH1, SLUG*) or Dunnett's T3 test (*SNAIL*). **H,** MDA-MB-231 cells with the restored expression of NSD3-long (NSD3-L) after stable knockdown of NSD3 isoforms (shNSD3) were treated with siRNAs against NOTCH1 for 24 hours, and changes in the expression levels of NOTCH1 and *SNAIL* were analyzed by immunoblotting (left) and qRT-PCR (right), respectively. Mean ± SD ($n = 3$). *P* values by one-way ANOVA with a *post hoc* LSD test. **I,** Schematic illustration of the promoter and transcription start site of *CDH1* gene locus containing the indicated binding motifs (top). ChIP analysis showing the fold enrichment of NICD1 and H3K27me3 at the promoter region of *CDH1* in NSD3-overexpressing MCF7 cells (bottom). Mean ± SD ($n = 3$). *P* values were calculated using two-sided Student *t* test.

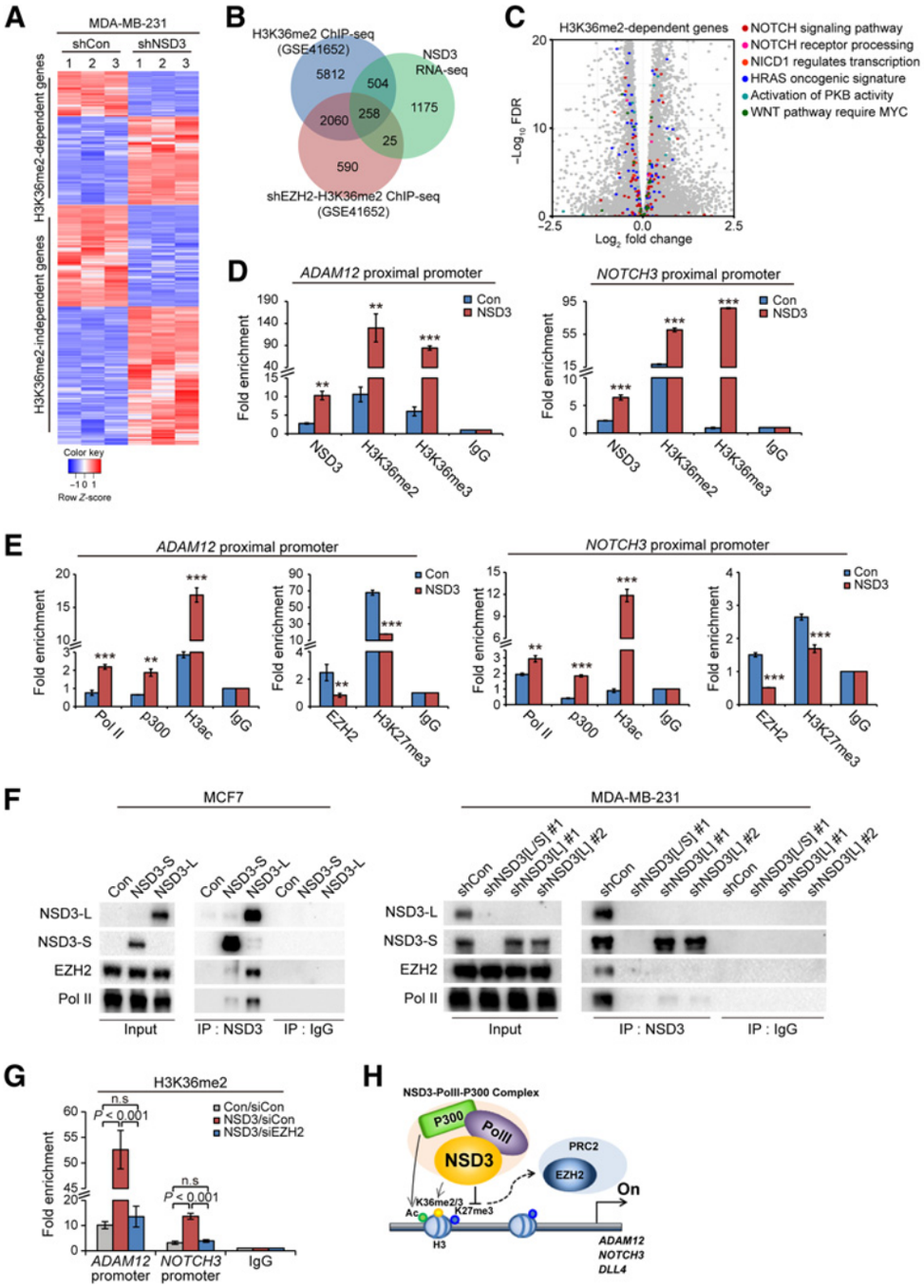

Figure 5.

Epigenetic regulation of ADAM12 and NOTCH3 by NSD3-p300-EZH2. **A,** Heatmap representing the differentially expressed genes between control (shCon) and NSD3-knockdown (shNSD3) groups in the RNA-seq analysis. ChIP-seq data for H3K36me2 in MDA-MB-231 cells (GSE41652) were used to sort the H3K36me2-dependent NSD3 target genes. **B,** The Venn diagram showing the number of overlapped genes among the results in the RNA-seq and ChIP-seq analysis. **C,** Volcano plot showing $\log_2$-fold changes of the mRNA expression of genes altered by NSD3-knockdown and the distribution of H3K36me2-dependent genes related to the indicated signaling pathways or functional categories. **D** and **E,** ChIP-qPCR analysis displaying the fold enrichment of indicated proteins and histone marks at the proximal promoter regions of *ADAM12* (left) and *NOTCH3* (right) in response to NSD3 expression. *P* values are based on two-sided Student *t* test. **, $P < 0.01$; ***, $P < 0.001$ versus Con. **F,** Cell lysates of NSD3-overexpressing MCF7 cells (left) and NSD3-knockdown MDA-MB-231 (right) were subjected to co-IP for analysis of interaction between the indicated proteins. shNSD3[L/S], shRNA for dually targeting NSD3-long and NSD3-short. shNSD3[L], shRNA targeting NSD3-long only. **G,** ChIP-qPCR analysis showing the fold enrichment of H3K36me2 at the indicated genomic regions after treatment of cells with EZH2 siRNA for 48 hours. Mean ± SD ($n = 3$). *P* values by one-way ANOVA with a *post hoc* LSD test (*ADAM12* promoter) or Welch's ANOVA with Dunnett T3 test (*NOTCH3* promoter). n.s., not significant. **H,** A proposed model for the epigenetic regulation of NOTCH and EMT-related genes by NSD3.

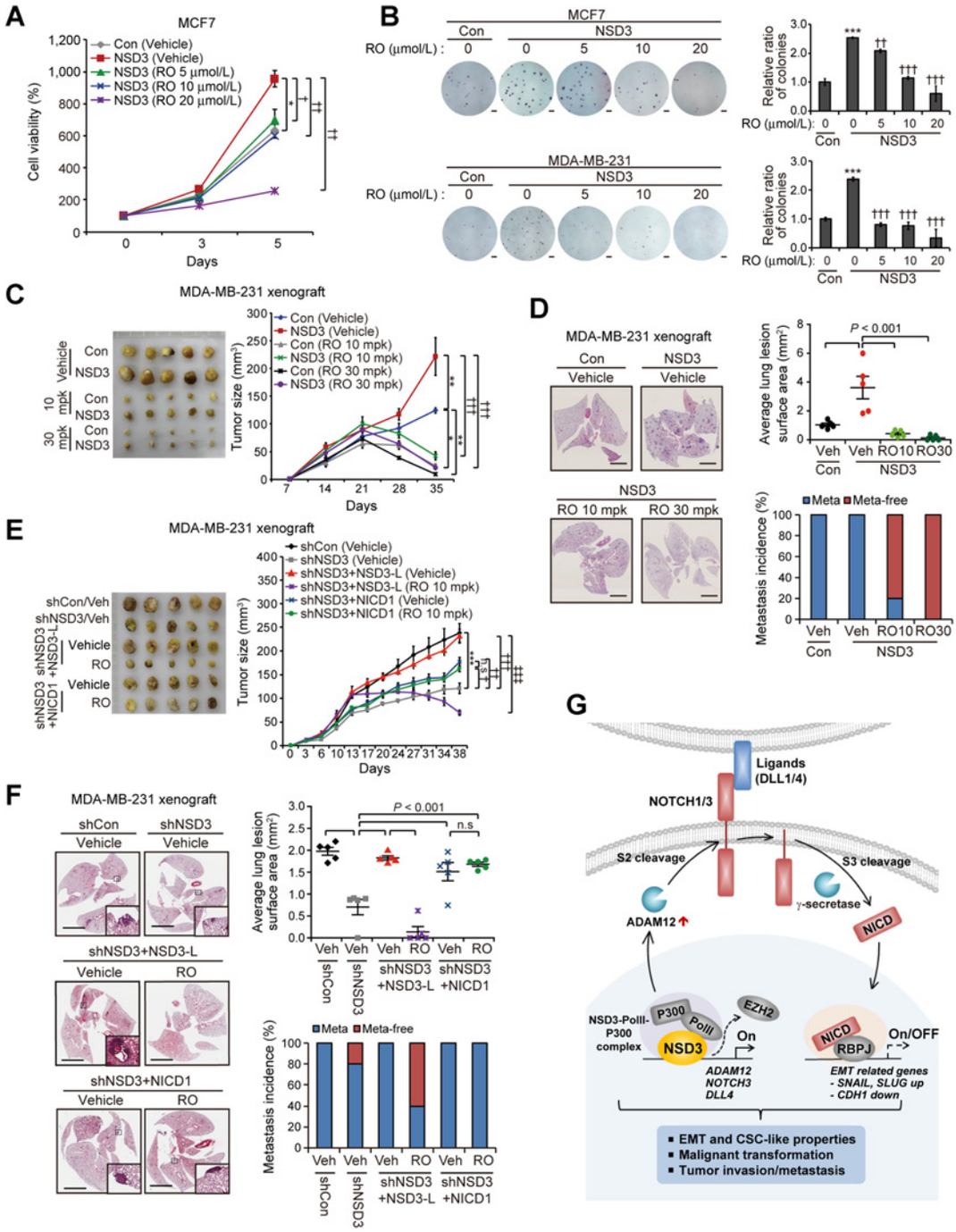

Figure 6.

Effect of NOTCH signaling inhibition on NSD3-induced tumor progression. **A** and **B,** Cells were treated with indicated doses of RO4929097 (RO) for 5 days and 21 days, and subjected to SRB assay (**A**) and colony forming assay (**B**), respectively. Mean ± SD ($n = 3$). *P* values were determined by RM ANOVA with Dunnett's T3 test (**A**) or one-way ANOVA (**B**) with a *post hoc* Tukey test. **C,** Effect of RO4929097 treatment on primary breast tumor growth in orthotopic xenograft mice bearing NSD3-overexpressing MDA-MB-231 tumors ($n = 5$ per group). The tumor growth curve (right) and images of tumors from xenografted mice after scarification (left) are shown. Mean ± SEM ($n = 5$). *P* values were calculated by RM ANOVA with a *post hoc* Tukey test. *, $P < 0.05$; **, $P < 0.01$ versus Con (Vehicle); †††, $P < 0.001$ versus NSD3 (Vehicle). mpk, mg/kg. **D,** Effect of RO4929097 treatment on the lung metastasis of breast cancer in mice bearing NSD3-overexpressing MDA-MB-231 tumors. Representative images of histologic analysis of lung metastasis (left), the area of lung metastatic lesions (top right), and incidence of metastasis (bottom right) are shown in the indicated groups of mice. Mean ± SEM ($n = 5$). *P* values were calculated by one-way ANOVA with a *post-hoc* LSD test (top right). Scale bars, 800 μm. Meta, metastasis; Meta-free, metastasis-free; Veh, vehicle. **E,** Effect of RO4929097 treatment on primary breast tumor growth in orthotopic xenograft mice harboring NSD3-knockdown MDA-MB-231 cells (shNSD3), with the restoration of either NSD3-long (shNSD3 + NSD3-L) or NICD1 (shNSD3 + NICD1). (*Continued on the following page.*)

they were broadly involved in the regulatory steps for NOTCH signaling cascades (**Fig. 4A** and **B**; Supplementary Fig. S7A). The main regulators of NOTCH receptor processing, including NOTCH receptor and ligands (*NOTCH3, DLL1*, and *DLL4*; ref. 28), and their downstream target genes (*HEY1, HEY2*, and *ADAM12*; refs. 28, 29), were altered by NSD3 (**Fig. 4C**; Supplementary Fig. S7B). Genes related to EMT, invasion and metastasis, including *CDH1* (4), *VIM* (4), and *ADAM12* (30, 31), were also identified as NSD3-target genes (**Fig. 4C**; Supplementary Fig. S7B). Given the GSEA results, we next investigated whether NSD3 affected the NOTCH receptor processing and signaling activity. The total amounts of the transmembrane (TM) domain and intracellular domain of NOTCH1 (NICD1), cleaved active forms of NOTCH1 receptor mediated by ADAM proteases and γ-secretases (28), were increased by NSD3, and subsequently the nuclear accumulation of NICD1 was facilitated in response to NSD3 expression (**Fig. 4D** and **E**; Supplementary Figs. S7C and S7D). Because of the transcriptional upregulation of *NOTCH3* by NSD3 (**Fig. 4C**; Supplementary Fig. S7B), both full length- and cleaved NOTCH3 protein expressions were increased by NSD3, and the cleaved NOTCH3 translocated into the nucleus (**Fig. 4D** and **E**; Supplementary Fig. S7D). ADAM family proteases, especially, ADAM10 and ADAM17, are known to play a key role in the cleavage and activation of NOTCH receptors (28). To determine whether ADAM12, a member of the ADAM family, has a similar function as ADAM10 and ADAM17 in the processing of NOTCH receptors, beyond its known role as a downstream of NOTCH signaling (29), the effect of ADAM12 on NSD3-induced NICD1 expression was examined. In NSD3-overexpressing MCF7 cells, transient knockdown of ADAM12 by siRNA abolished the NSD3-induced NICD1 accumulation (**Fig. 4F**), suggesting that ADAM12 may trigger NOTCH receptor cleavage. Particularly, dual knockdown of NSD3 isoforms and NSD3-long-specific knockdown showed similar effects on changes in the expression levels of NOTCH regulators and the amount of NICD1 (Supplementary Figs. S7E and S7F), suggesting that NSD3-long may modulate NOTCH signaling pathway in an independent manner of NSD3-short.

The translocation of NICDs into the nucleus is generally involved in the activation of target gene transcription (28), and several EMT-inducing transcription factors (EMT-TF), such as Snail and Slug, were identified as downstream targets of NOTCH signaling (32–34). In NSD3-overexpressing MCF7 cell lines, the treatment with RO4929097, a GSI (28, 35), reversed the expression patterns of EMT-TFs and E-cadherin at the transcriptional levels (**Fig. 4G**). Likewise, NOTCH1 siRNA treatment inhibited NSD3-induced Snail expression (**Fig. 4H**). Interestingly, NICD1 was also directly recruited to the proximal promoter region of *CDH1*, where EMT-TFs and EZH2 are known to bind (4, 36), and facilitated H3K27me3 upon NSD3 overexpression (**Fig. 4I**), implicating the potential role of polycomb-repressive complex (PRC)-2 in the NOTCH-dependent transcriptional repression as previously reported (37). Taken together, these data indicate that the molecular changes into EMT by NSD3 are mediated by NOTCH signaling activation.

NSD3 induces H3K36 methylation-dependent transcription of NOTCH-related genes in collaboration with EZH2 and polymerase II

To further investigate the functional role of NSD3 catalytic activity, the RNA-seq results were compared with ChIP-seq data for H3K36me2 (GSE41652) to distinguish the H3K36me2-dependent NSD3-target genes. Of the total 1,962 genes altered by NSD3 knockdown (>1.5-fold, $P < 0.05$), approximately 40% of the genes were overlapped with H3K36me2-dependent genes (**Fig. 5A**; Supplementary Fig. S7G). In addition, in agreement with the GSEA showing the association between NSD3 and EZH2 target genes (**Fig. 4A**), nearly 30% of the H3K36me2-enriched NSD3 targets were EZH2-dependent in the comparison analysis of RNA-seq and ChIP-seq data (**Fig. 5B**), implying a reciprocal relationship between H3K27me3 and H3K36me2. In particular, among the NSD3-target genes involved in EMT/CSC-associated signaling pathways, many of the genes related to NOTCH signaling, such as NOTCH receptors, ligands, and ADAM12, were H3K36me2-dependent (**Fig. 5C**; Supplementary Fig. S7H). Accordingly, ChIP analyses showed that NSD3 was recruited to the proximal promoter or gene body regions of *NOTCH3, ADAM12*, and *DLL4*, and facilitated the H3K36me2 and H3K36me3 at these regions, to enhance the transcription of these genes (**Fig. 5D**; Supplementary Fig. S7I). Furthermore, histone H3 acetylation (H3ac) was increased, whereas H3K27me3 levels were decreased at the regions, that were accompanied by co-recruitment of p300 acetyltransferase and RNA polymerase II (PolII) and dissociation of EZH2 (**Fig. 5E**). Interestingly, co-immunoprecipitation analysis indicated that NSD3 interacts with PolII and EZH2, and the bindings were preferential to NSD3-long compared with those of NSD3-short effect in MCF7 cells (**Fig. 5F**, left). Similar results were shown in MDA-MB-231 cells with NSD3-long-specific knockdown (**Fig. 5F**, right). Furthermore, transient knockdown of EZH2 impaired H3K36 methylation at the promoter regions of *ADAM12* and *NOTCH3* (**Fig. 5G**), implying the EZH2-dependent NSD3 recruitment to the target loci. Taken together, these data suggest that NSD3-long interacts with PolII and EZH2 to recognize and inhibit EZH2-dependent H3K27me3 and to form a transcriptionally active complex with PolII and p300 at the promoter regions of NOTCH-related genes for H3K36me2/3-dependent gene expression (**Fig. 5H**), suggesting the crucial role of NSD3 HMT activity in modulating the NOTCH signaling.

Targeting NOTCH signaling is required for inhibiting NSD3-induced metastatic progression in breast cancer

To determine the therapeutic availability of NOTCH inhibition in aggressive breast cancer with high NSD3 expression, the effect of

(*Continued.*) The tumor growth curve (right) and images of tumors from xenografted mice after scarification (left) are shown. Mean ± SEM ($n = 5$ mice per group). *P* values were determined by RM ANOVA with a *post hoc* LSD test. ***, $P < 0.001$ versus shCon (Vehicle); †, $P < 0.05$; ††, $P < 0.01$; †††, $P < 0.001$ versus shNSD3 (Vehicle); ‡‡‡, $P < 0.001$ versus shNSD3 + NSD3-L (Vehicle). mpk, mg/kg; n.s., not significant. **F,** Analysis of the effect of NOTCH signaling inhibition on the lung metastasis of breast cancer in mice bearing NSD3-knockdown MDA-MB-231 tumors, followed by rescued expression of NSD3-long or NICD1. Representative images of histologic analysis of lung metastasis (left), dot plot showing the area of lung metastatic lesions (top right), and incidence of metastasis (bottom right) in the indicated groups of mice. Mean ± SEM ($n = 5$). *P* values by one-way ANOVA with a *post hoc* LSD test (top right). Scale bars, 800 μm. **G,** A proposed model for the regulation of EMT-CSC-metastasis via the epigenetic modulation of NOTCH signaling by NSD3. For the transactivation of genes related to NOTCH signaling activation, including *ADAM12* and *NOTCH3*, NSD3 interaction with EZH2 and PolII leads to the recruitment of NSD3 to target loci marked by H3K27me3, dissociates EZH2 from the regions, and facilitates H3K36 methylation and PolII recruitment at these regions. The increased ADAM12 expression by NSD3 promotes the cleavage of NOTCH1 and NOTCH3 and nuclear accumulation of these receptor, thus leading to NOTCH signaling-dependent upregulation of EMT inducers, Snail and Slug, and downregulation of epithelial marker E-cadherin. The activation of NOTCH signaling mediates NSD3-induced tumor initiation, progression, and metastasis.

RO4929097, a GSI used in clinical trials (28, 35), on NSD3-induced tumor growth and metastasis was investigated. The anchorage-dependent and -independent cancer cell growth accelerated by NSD3 overexpression was inhibited by RO4929097 in a dose-dependent manner, in MCF7 and MDA-MB-231 cell lines harboring low and moderate expression levels of NSD3, respectively (**Fig. 6A** and **B**). Consistently, in an orthotopic xenograft, NSD3-induced tumor growth was inhibited by treatment with GSI, and the mice harboring NSD3-overexpressing MDA-MB-231 tumors showed higher sensitivity to the GSI than the control mice (**Fig. 6C**; Supplementary Figs. S8A and S8B). We further explored the anticancer effect of GSI against NSD3-induced tumor invasion and metastasis. In MCF7 cells with low invasive capacity, the increased migration and invasion by NSD3 overexpression were impaired upon GSI treatment (Supplementary Fig. S8C). NSD3 overexpression was also able to facilitate the migration and invasion capacities in MDA-MB-231 cells with highly invasive and metastatic potential, and these effects were inhibited by GSI treatment (Supplementary Fig. S8D). Consistent with the *in vitro* results, an *in vivo* breast tumor metastasis model by tail vein injection of NSD3-overexpressing MDA-MB-231 cells into mice showed that NSD3-induced lung metastasis of breast tumors was prohibited by the administration of GSI (**Fig. 6D**). Furthermore, the restoration of NSD3-long or NICD1 in MDA-MB-231 tumors with stable knockdown of NSD3 isoforms rescued inhibitory effect of NSD3 knockdown on primary tumor growth and metastasis *in vivo*, as well as migration and invasion *in vitro* (**Fig. 6E** and **F**; Supplementary Figs. S8E–S8G). In addition, the recovery of these effects by NSD3-long was abolished by the treatment with RO4929097, indicating the NOTCH signaling-dependent oncogenic potential of NSD3-long. We also confirmed that the anti-tumor effect of RO4929097 resulted from NOTCH1 cleavage by γ-secretase, as constitutive NICD1 overexpression in NSD3-knockdown MDA-MB-231 tumors showed refractory to GSI (**Fig. 6E** and **F**; Supplementary Figs. S8E–S8G). Taken together with our *in vitro* and *in vivo* data, we concluded that NSD3-induced CSC and EMT properties and tumor metastasis are mediated by NOTCH signaling, and that targeting NOTCH signaling is required for the treatment of aggressive breast cancer with high NSD3 expression/amplification.

Discussion

This study demonstrates the crucial role of the HMT activity of NSD3 in breast tumor initiation and metastasis. Comprehensive analyses of the clinical significance and molecular function of NSD3 indicated that high NSD3 expression is a poor prognostic marker associated with tumor relapse and metastasis caused by the acquisition of CSC and EMT phenotypes. As an HMT activity-dependent mechanism of NSD3, we found that NSD3 forms a transcriptional active complex with p300 HAT and PolII, facilitates H3K36me2/3 and H3ac, and inhibits EZH2-dependent H3K27me3 at the proximal promoter regions of genes involved in the NOTCH pathway, via the preferential interaction of NSD3-long with PolII and EZH2. This leads to NOTCH receptor cleavage and signaling activation and subsequent CSC and EMT (**Fig. 6G**). Therefore, NSD3 might serve as a new epigenetic regulator for breast cancer development and progression to a more aggressive status, suggesting NSD3 to be a therapeutic target for metastatic breast cancer.

Our data provide strong evidence for the central role of NSD3 isoforms as cancer drivers of 8p11–12 amplicon in human cancers. The 8p11–12 amplicon has been implicated in high-grade and Ki-67 proliferative index, recurrence, and poor prognosis in breast cancer (38–40); however, it remains controversial which of the genes at 8p11–12 dominantly function as strong cancer drivers (39, 41). Accumulating studies for genetic analysis of the 8p11–12 amplicon and whole-genome sequencing of human cancers have suggested *NSD3* as a candidate driver gene in various types of solid tumors, including breast cancer (14, 39, 41). In agreement with these studies, Either and colleagues found that the NSD3-short isoform has the highest transforming ability among the genes in the 8p11–12 amplicon in a cell line model (23), and more recently, they proved the development of hyperplasia and tumors in MMTV-driven NSD3 transgenic mice (42). Although these data suggest a key role of NSD3 in breast tumorigenesis, there is little evidence to support the oncogenic function of NSD3 *in vitro* and *in vivo*, remaining elusive which isoform of NSD3 has dominant functions in breast tumor development. To our knowledge, the present *in vitro* and *in vivo* data demonstrating the induction of cancer stemness, malignant transformation, EMT, and metastasis by NSD3-long are the first direct evidence to support the notion that NSD3-long plays a crucial role as a key cancer driver in the epigenetic regulation of breast cancer initiation and progression. Because NSD3-short was also involved in acquiring CSC and EMT phenotype in our data, it is likely that the overexpression of both NSD3 isoforms by 8p11–12 amplification may synergistically or independently promote breast tumor initiation and progression.

Furthermore, our findings suggest a new indication of NOTCH inhibitors in the treatment of aggressive breast cancer with the 8p11–12 amplicon by identifying the new epigenetic regulatory mechanism of NOTCH signaling by NSD3-long. Given the importance of NOTCH signaling in modulating the self-renewal of CSCs, as well as EMT and metastasis, inhibitors for NOTCH signaling, such as GSIs, have emerged as CSC-directed therapies or new treatment strategies for metastatic cancers in preclinical and clinical models (35, 43). However, NOTCH signaling also has a tumor-suppressive function (44), raising the need to understand the context-dependent role of NOTCH signaling for personalized cancer therapy due to the paradoxical role. On the basis of our findings, it could be suggested that 8p11–12 amplified tumors may possess highly tumorigenic and aggressive potential because of hyperactivation of oncogenic NOTCH signaling by NSD3-long; thus, NOTCH inhibition may be required for treatment of human cancers with the 8p11–12 amplicon.

Of note, NSD3 HMT activity is critical for breast cancer development and metastatic progression, which supports a key role of epigenetic regulation in the metastatic progression, suggesting an antimetastatic epigenetic therapy for aggressive breast cancer. Despite improvements in breast cancer treatment, distant metastasis of breast cancer is a major cause of cancer-related death and is still regarded as incurable with currently available therapies (1). Our data showing the specific role of NSD3-dependent H3K36 methylation in the regulation of NOTCH signaling-mediated EMT/CSCs and the inhibitory effect of NSD3-knockdown for primary and metastatic breast tumor suggest that NSD3-targeted epigenetic therapy could be a promising strategy for the treatment of advanced breast cancer. Because the pharmacologic inhibition of NSD3 is currently unavailable due to lack of appropriate specific inhibitors for H3K36 methylation of the NSD family, further research is still needed for development of a selective inhibitor targeting NSD3 catalytic activity to determine the therapeutic availability of NSD3 inhibition in the treatment of aggressive and metastatic cancers.

Our data also establish a new molecular mechanism underlying the regulation of gene expression by NSD3-induced H3K36 methylation. Although H3K36me2/3 generally marks gene bodies rather than the upstream region of genes (45, 46), a previous report showed that NSD1

binds the proximal gene promoter regions and recruits PolII to the target loci during transcription initiation and elongation (47). NSD3 was also reported to be preferentially recruited to promoter regions, despite the highly enriched H3K36me3 levels at the gene bodies (48). In agreement with these results, our data suggest that NSD3 can recognize the proximal promoter regions of specific target genes involved in NOTCH signaling and induce H3K36me2/3 at the regions to facilitate active transcription in collaboration with PolII and p300 HAT. Likewise, NSD3 was identified as a component of the LSD2-associated complex consisting of transcription machinery factors, including PolII, P-TEFb, and CDK9 (49). Therefore, it can be speculated that NSD3 may play a key role in the initiation of transcription as a main component for PolII/p300-associated transcription complex.

Furthermore, it is notable that NSD3-long, but not NSD3-short, preferentially binds to PolII and EZH2 proteins, suggesting a possible mechanism for NSD3-long-specific recruitment to target chromatin. It is likely that HMTs for H3K36, which do not possess the binding ability to a sequence-specific DNA, are guided by their interacting partners, such as transcription factors, transcription-initiation machinery, and other histone-modifying enzymes and chromatin remodeling factors (45). NSD3-short, which contains only the PWWP domain, is guided to the Myc super-enhancer regions via the interaction with BRD4-CHD8 (22) and Myc (50); however, little is known about the protein interactions in a specific manner to NSD3-long, possessing more functional domains, including PHD and SET. On the basis of our results, we assume that the binding ability of NSD3-long to EZH2 and PolII may guide NSD3 to specific target loci marked by H3K27me3 or PolII. Therefore, NSD3-long may have distinct binding patterns of protein complexes and target chromatins from those of NSD3-short via its c-terminal domains containing PHD motifs, which are absent in NSD3-short. Thus, both NSD3 isoforms might function independently or cooperatively in modulating the gene expression and biological processes. Further investigation is required to fully elucidate the functional interdependence between these two isoforms.

In conclusion, our study delineates the crucial role of NSD3 in breast tumor initiation and metastasis that was closely linked to the H3K36me2/3-dependent NOTCH signaling activation, suggesting NSD3 to be a new biomarker for aggressive and metastatic breast cancer.

Authors' Disclosures

No disclosures were reported.

Authors' Contributions

G.-Y. Jeong: Data curation, validation, investigation, writing-original draft. **M.K. Park:** Data curation, validation, investigation, writing-original draft. **H.-J. Choi:** Data curation, validation, investigation. **H.W. An:** Validation, investigation. **Y.-U. Park:** Validation, investigation. **H-J. Choi:** Validation, investigation. **J. Park:** Validation, investigation. **H.-Y. Kim:** Validation, investigation. **T. Son:** Validation, investigation. **H. Lee:** Validation, investigation. **K.-W. Min:** Validation, investigation. **Y-H. Oh:** Validation, investigation. **J.-Y. Lee:** Conceptualization, supervision, writing-original draft, writing-review and editing. **G. Kong:** Conceptualization, supervision, funding acquisition, writing-review and editing.

Acknowledgments

This work was supported by the National Research Foundation of Korea (NRF) grants funded by the Korean government (No. 2019R1A2C3006305 to G. Kong).

The costs of publication of this article were defrayed in part by the payment of page charges. This article must therefore be hereby marked *advertisement* in accordance with 18 U.S.C. Section 1734 solely to indicate this fact.

Received January 31, 2020; revised July 31, 2020; accepted September 18, 2020; published first September 23, 2020.

References

1. Arnedos M, Vicier C, Loi S, Lefebvre C, Michiels S, Bonnefoi H, et al. Precision medicine for metastatic breast cancer—limitations and solutions. Nat Rev Clin Oncol 2015;12:693–704.
2. Beck B, Blanpain C. Unravelling cancer stem cell potential. Nat Rev Cancer 2013;13:727–38.
3. Brabletz T, Kalluri R, Nieto MA, Weinberg RA. EMT in cancer. Nat Rev Cancer 2018;18:128–34.
4. Dongre A, Weinberg RA. New insights into the mechanisms of epithelial-mesenchymal transition and implications for cancer. Nat Rev Mol Cell Biol 2019;20:69–84.
5. Mani SA, Guo W, Liao MJ, Eaton EN, Ayyanan A, Zhou AY, et al. The epithelial-mesenchymal transition generates cells with properties of stem cells. Cell 2008;133:704–15.
6. Guo W, Keckesova Z, Donaher JL, Shibue T, Tischler V, Reinhardt F, et al. Slug and Sox9 cooperatively determine the mammary stem cell state. Cell 2012;148:1015–28.
7. Ye X, Tam WL, Shibue T, Kaygusuz Y, Reinhardt F, Ng Eaton E, et al. Distinct EMT programs control normal mammary stem cells and tumour-initiating cells. Nature 2015;525:256–60.
8. Lee JY, Kong G. Roles and epigenetic regulation of epithelial-mesenchymal transition and its transcription factors in cancer initiation and progression. Cell Mol Life Sci 2016;73:4643–60.
9. Tam WL, Weinberg RA. The epigenetics of epithelial-mesenchymal plasticity in cancer. Nat Med 2013;19:1438–49.
10. Chang CJ, Yang JY, Xia W, Chen CT, Xie X, Chao CH, et al. EZH2 promotes expansion of breast tumor initiating cells through activation of RAF1-beta-catenin signaling. Cancer Cell 2011;19:86–100.
11. Cho MH, Park JH, Choi HJ, Park MK, Won HY, Park YJ, et al. DOT1L cooperates with the c-Myc-p300 complex to epigenetically derepress CDH1 transcription factors in breast cancer progression. Nat Commun 2015;6:7821.
12. Dong C, Wu Y, Yao J, Wang Y, Yu Y, Rychahou PG, et al. G9a interacts with Snail and is critical for Snail-mediated E-cadherin repression in human breast cancer. J Clin Invest 2012;122:1469–86.
13. Wu Y, Wang Y, Yang XH, Kang T, Zhao Y, Wang C, et al. The deubiquitinase USP28 stabilizes LSD1 and confers stem-cell-like traits to breast cancer cells. Cell Rep 2013;5:224–36.
14. Chen Y, McGee J, Chen X, Doman TN, Gong X, Zhang Y, et al. Identification of druggable cancer driver genes amplified across TCGA datasets. PLoS One 2014;9:e98293.
15. Liu L, Kimball S, Liu H, Holowatyj A, Yang ZQ. Genetic alterations of histone lysine methyltransferases and their significance in breast cancer. Oncotarget 2015;6:2466–82.
16. Li Y, Trojer P, Xu CF, Cheung P, Kuo A, Drury WJ 3rd, et al. The target of the NSD family of histone lysine methyltransferases depends on the nature of the substrate. J Biol Chem 2009;284:34283–95.
17. Angrand PO, Apiou F, Stewart AF, Dutrillaux B, Losson R, Chambon P. NSD3, a new SET domain-containing gene, maps to 8p12 and is amplified in human breast cancer cell lines. Genomics 2001;74:79–88.
18. Tonon G, Wong KK, Maulik G, Brennan C, Feng B, Zhang Y, et al. High-resolution genomic profiles of human lung cancer. Proc Natl Acad Sci U S A 2005;102:9625–30.
19. Kang D, Cho HS, Toyokawa G, Kogure M, Yamane Y, Iwai Y, et al. The histone methyltransferase Wolf-Hirschhorn syndrome candidate 1-like 1 (WHSC1L1) is involved in human carcinogenesis. Genes Chromosomes Cancer 2013;52:126–39.
20. Mahmood SF, Gruel N, Nicolle R, Chapeaublanc E, Delattre O, Radvanyi F, et al. PPAPDC1B and WHSC1L1 are common drivers of the 8p11–12 amplicon, not

only in breast tumors but also in pancreatic adenocarcinomas and lung tumors. Am J Pathol 2013;183:1634–44.
21. Stec I, van Ommen GJ, den Dunnen JT. WHSC1L1, on human chromosome 8p11.2, closely resembles WHSC1 and maps to a duplicated region shared with 4p16.3. Genomics 2001;76:5–8.
22. Shen C, Ipsaro JJ, Shi JW, Milazzo JP, Wang E, Roe JS, et al. NSD3-short is an adaptor protein that couples BRD4 to the CHD8 chromatin remodeler. Mol Cell 2015;60:847–59.
23. Yang ZQ, Liu G, Bollig-Fischer A, Giroux CN, Ethier SP. Transforming properties of 8p11–12 amplified genes in human breast cancer. Cancer Res 2010;70:8487–97.
24. Choi HJ, Jin S, Cho H, Won HY, An HW, Jeong GY, et al. CDK12 drives breast tumor initiation and trastuzumab resistance via WNT and IRS1-ErbB-PI3K signaling. EMBO Rep 2019:e48058.
25. Al-Hajj M, Wicha MS, Benito-Hernandez A, Morrison SJ, Clarke MF. Prospective identification of tumorigenic breast cancer cells. Proc Natl Acad Sci U S A 2003;100:3983–8.
26. Scheel C, Weinberg RA. Cancer stem cells and epithelial-mesenchymal transition: concepts and molecular links. Semin Cancer Biol 2012;22:396–403.
27. Ye X, Brabletz T, Kang Y, Longmore GD, Nieto MA, Stanger BZ, et al. Upholding a role for EMT in breast cancer metastasis. Nature 2017;547:E1–E3.
28. Andersson ER, Lendahl U. Therapeutic modulation of Notch signalling–are we there yet? Nat Rev Drug Discov 2014;13:357–78.
29. Diaz B, Yuen A, Iizuka S, Higashiyama S, Courtneidge SA. Notch increases the shedding of HB-EGF by ADAM12 to potentiate invadopodia formation in hypoxia. J Cell Biol 2013;201:279–92.
30. Eckert MA, Santiago-Medina M, Lwin TM, Kim J, Courtneidge SA, Yang J. ADAM12 induction by Twist1 promotes tumor invasion and metastasis via regulation of invadopodia and focal adhesions. J Cell Sci 2017;130:2036–48.
31. Ruff M, Leyme A, Le Cann F, Bonnier D, Le Seyec J, Chesnel F, et al. The Disintegrin and Metalloprotease ADAM12 Is Associated with TGF-beta-Induced Epithelial to Mesenchymal Transition. PLoS One 2015;10:e0139179.
32. Sahlgren C, Gustafsson MV, Jin S, Poellinger L, Lendahl U. Notch signaling mediates hypoxia-induced tumor cell migration and invasion. Proc Natl Acad Sci U S A 2008;105:6392–7.
33. Timmerman LA, Grego-Bessa J, Raya A, Bertran E, Perez-Pomares JM, Diez J, et al. Notch promotes epithelial-mesenchymal transition during cardiac development and oncogenic transformation. Genes Dev 2004;18:99–115.
34. Niessen K, Fu Y, Chang L, Hoodless PA, McFadden D, Karsan A. Slug is a direct Notch target required for initiation of cardiac cushion cellularization. J Cell Biol 2008;182:315–25.
35. Tolcher AW, Messersmith WA, Mikulski SM, Papadopoulos KP, Kwak EL, Gibbon DG, et al. Phase I study of RO4929097, a gamma secretase inhibitor of Notch signaling, in patients with refractory metastatic or locally advanced solid tumors. J Clin Oncol 2012;30:2348–53.
36. Cao Q, Yu J, Dhanasekaran SM, Kim JH, Mani RS, Tomlins SA, et al. Repression of E-cadherin by the polycomb group protein EZH2 in cancer. Oncogene 2008;27:7274–84.
37. Han X, Ranganathan P, Tzimas C, Weaver KL, Jin K, Astudillo L, et al. Notch represses transcription by PRC2 recruitment to the ternary complex. Mol Cancer Res 2017;15:1173–83.
38. Gelsi-Boyer V, Orsetti B, Cervera N, Finetti P, Sircoulomb F, Rouge C, et al. Comprehensive profiling of 8p11–12 amplification in breast cancer. Mol Cancer Res 2005;3:655–67.
39. Ray ME, Yang ZQ, Albertson D, Kleer CG, Washburn JG, Macoska JA, et al. Genomic and expression analysis of the 8p11–12 amplicon in human breast cancer cell lines. Cancer Res 2004;64:40–7.
40. Yang ZQ, Streicher KL, Ray ME, Abrams J, Ethier SP. Multiple interacting oncogenes on the 8p11-p12 amplicon in human breast cancer. Cancer Res 2006;66:11632–43.
41. Garcia MJ, Pole JC, Chin SF, Teschendorff A, Naderi A, Ozdag H, et al. A 1 Mb minimal amplicon at 8p11-12 in breast cancer identifies new candidate oncogenes. Oncogene 2005;24:5235–45.
42. Turner-Ivey B, Smith EL, Rutkovsky AC, Spruill LS, Mills JN, Ethier SP. Development of mammary hyperplasia, dysplasia, and invasive ductal carcinoma in transgenic mice expressing the 8p11 amplicon oncogene NSD3. Breast Cancer Res Treat 2017;164:349–58.
43. Zhao Y, Dong Q, Li J, Zhang K, Qin J, Zhao J, et al. Targeting cancer stem cells and their niche: perspectives for future therapeutic targets and strategies. Semin Cancer Biol 2018;53:139–55.
44. Krishna BM, Jana S, Singhal J, Horne D, Awasthi S, Salgia R, et al. Notch signaling in breast cancer: from pathway analysis to therapy. Cancer Lett 2019;461:123–31.
45. Wagner EJ, Carpenter PB. Understanding the language of Lys36 methylation at histone H3. Nat Rev Mol Cell Biol 2012;13:115–26.
46. Barski A, Cuddapah S, Cui K, Roh TY, Schones DE, Wang Z, et al. High-resolution profiling of histone methylations in the human genome. Cell 2007;129:823–37.
47. Lucio-Eterovic AK, Singh MM, Gardner JE, Veerappan CS, Rice JC, Carpenter PB. Role for the nuclear receptor-binding SET domain protein 1 (NSD1) methyltransferase in coordinating lysine 36 methylation at histone 3 with RNA polymerase II function. Proc Natl Acad Sci U S A 2010;107:16952–7.
48. Rahman S, Sowa ME, Ottinger M, Smith JA, Shi Y, Harper JW, et al. The Brd4 extraterminal domain confers transcription activation independent of pTEFb by recruiting multiple proteins, including NSD3. Mol Cell Biol 2011;31:2641–52.
49. Fang R, Barbera AJ, Xu Y, Rutenberg M, Leonor T, Bi Q, et al. Human LSD2/KDM1b/AOF1 regulates gene transcription by modulating intragenic H3K4me2 methylation. Mol Cell 2010;39:222–33.
50. Li Z, Ivanov AA, Su R, Gonzalez-Pecchi V, Qi Q, Liu S, et al. The OncoPPi network of cancer-focused protein-protein interactions to inform biological insights and therapeutic strategies. Nat Commun 2017;8:14356.